LETTER • OPEN ACCESS

Multi-temporal image analysis of historical aerial photographs and recent satellite imagery reveals evolution of water body surface area and polygonal terrain morphology in Kobuk Valley National Park, Alaska

View the article online for updates and enhancements.

Multi-temporal image analysis of historical aerial photographs and recent satellite imagery reveals evolution of water body surface area and polygonal terrain morphology in Kobuk Valley National Park, Alaska

Marius Necsoiu[1], Cynthia L Dinwiddie[1], Gary R Walter[1], Amy Larsen[2] and Stuart A Stothoff[1]

[1] Southwest Research Institute®, Geosciences and Engineering Division, 6220 Culebra Road, San Antonio, TX, USA
[2] US National Park Service, 4175 Geist Road, Fairbanks, AK, USA

E-mail: mnecsoiu@swri.org

Abstract
Multi-temporal image analysis of very-high-resolution historical aerial and recent satellite imagery of the Ahnewetut Wetlands in Kobuk Valley National Park, Alaska, revealed the nature of thaw lake and polygonal terrain evolution over a 54-year period of record comprising two 27-year intervals (1951–1978, 1978–2005). Using active-contouring-based change detection, high-precision orthorectification and co-registration and the normalized difference index, surface area expansion and contraction of 22 shallow water bodies, ranging in size from 0.09 to 179 ha, and the transition of ice-wedge polygons from a low- to a high-centered morphology were quantified. Total surface area decreased by only 0.4% during the first time interval, but decreased by 5.5% during the second time interval. Twelve water bodies (ten lakes and two ponds) were relatively stable with net surface area decreases of ≤10%, including four lakes that gained area during both time intervals, whereas ten water bodies (five lakes and five ponds) had surface area losses in excess of 10%, including two ponds that drained completely. Polygonal terrain remained relatively stable during the first time interval, but transformation of polygons from low- to high-centered was significant during the second time interval.

1. Introduction

Subarctic wetlands are transitional areas between hundreds of thousands of shallow ponds and lakes and the surrounding
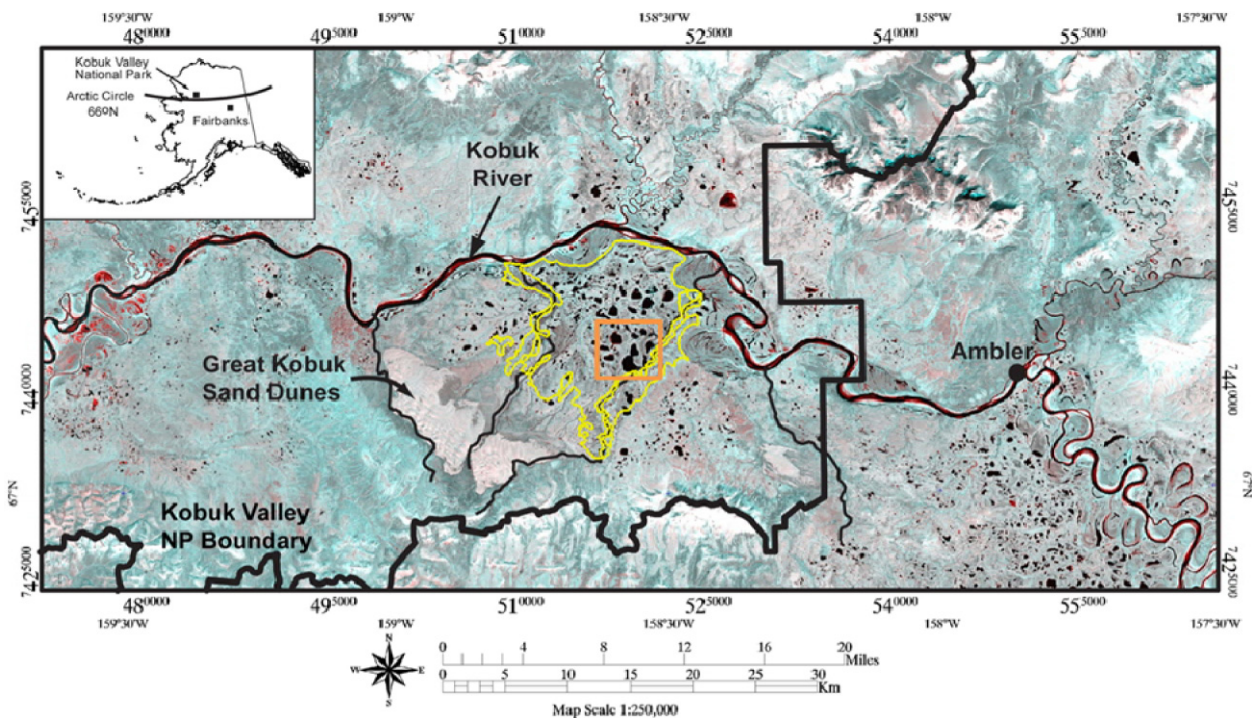
Figure 1. Context image for the Ahnewetut Wetlands study area. Inset provides geographic context. Yellow contour represents the Ahnewetut Wetlands boundary (Swanson 2001) within Kobuk Valley National Park (thick black contour). Study area is bounded by orange rectangle. Graphic created using the NIR channel (Band 4) of Landsat ETM+, acquired 30 August 2002 (displayed in red channel) and Landsat TM, acquired 6 July 1985 (displayed in green and blue channels). Data source: Global Land Cover Facility.

terrestrial environment; they are particularly sensitive to minor shifts in the hydrologic cycle (e.g., Chapin *et al* 2006; Prowse *et al* 2006; Schindler and Smol 2006) and thermal regime. Wetlands are highly productive ecosystems that provide surface water and water filtration, flood protection, groundwater recharge through open taliks, carbon storage, and wildlife migration routes and habitat for moose, waterfowl, furbearers, and subsistence (Berkes and Jolly 2001). A warming global climate is expected to accelerate the exchange of mass and energy between the reservoirs that together comprise the regional hydrologic cycle. In recent decades, air and ground temperatures in the continuous and most of the discontinuous permafrost zones in Alaska have increased (e.g., Hinzman *et al* 2005; Osterkamp 2007). Warming in interior Alaska will affect snowfall and rainfall patterns, permafrost stability and distribution, surface water and groundwater hydrology, water quality, and vegetation dynamics. Pore-occluding permafrost, segregated ice lenses, and massive wedge ice inhibit infiltration and vadose zone drainage (Ford and Bedford 1987). Loss of permafrost and massive ice will increase both the storage capacity and hydraulic conductivity of shallow subsurface reservoirs, and will result in greater connectivity between surface water and groundwater, likely reducing the size and number of shallow subarctic ponds and lakes, altering adjacent drainage networks, and affecting ecosystem services provided by subarctic wetlands.

Extensive changes to shallow ponds and lakes, both a consequence and indicator of permafrost degradation (Osterkamp and Romanovsky 1999), vary along an evolutionary continuum from initial expansion of the number or size of shallow ponds and lakes (Smith *et al* 2005) to rapid drainage and significant permanent loss of surface water (Marsh *et al* 2009) and related changes in water body surface area (Yoshikawa and Hinzman 2003, Smith *et al* 2005, Riordan *et al* 2006, Roach *et al* 2011). Based on recent results of a broad survey of 15 lake pairs that exhibit opposing contraction/expansion behaviors, Roach *et al* (2011) posit that terrestrialization and thermokarsting are the most likely mechanisms causing simultaneous lake area contraction and expansion, with both mechanisms enhanced by recent climate warming.

Important information about the physical and hydrological conditions that drive wetland lake ecosystem dynamics in remote Kobuk Valley National Park (KOVA), northwestern interior Alaska, is lacking due to limited funding and study. Under the framework of the US National Park Service's vital signs monitoring program, park scientists recently observed the effects of local warming on permafrost instability within the Kobuk lowlands, including numerous catastrophically drained ponds and lakes (Larsen and Kristenson 2010). Larsen and Kristenson (2010) identified several examples of old lake coalescence, and both old and recent catastrophic channel breaches.

Various image analysis technologies have been used to quantify water body surface area changes occurring in thermokarst wetlands (e.g., Kaab *et al* 1997, Yoshikawa and Hinzman 2003, Grosse *et al* 2005, Jorgenson *et al* 2006, Riordan *et al* 2006, Mars and Houseknecht 2007, Hinkel *et al* 2007, Plug *et al* 2008, Marsh *et al* 2009, Sannel and Brown 2010, Jones *et al* 2011, Sannel and Kuhry 2011). Analyses of high-resolution aerial imagery generally use fully manual
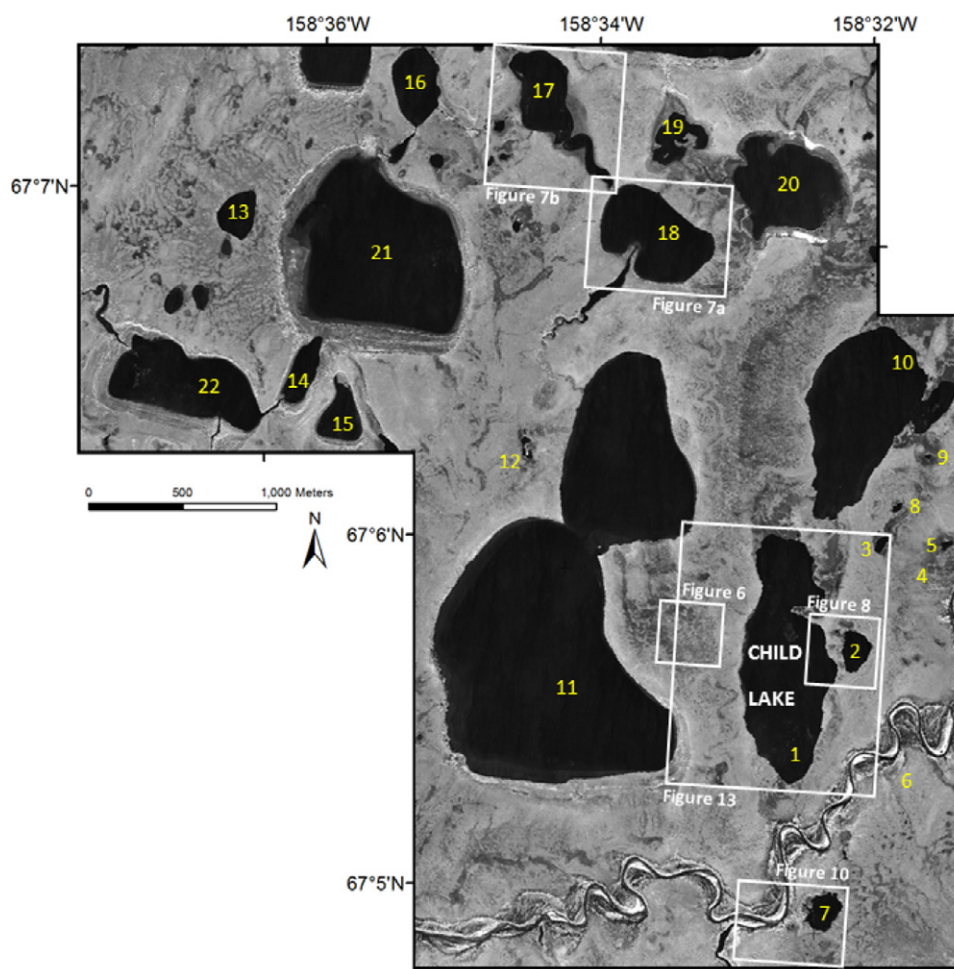
Figure 2. 2005 QuickBird context image of ponds, lakes, and polygonal terrain. Regions and features identified by inset box and figure or feature number are discussed in detail later in this paper.

approaches to water body surface area contouring, with the exceptions of Hinkel *et al* (2007) and Jones *et al* (2009, 2011). Semi-automated boundary delineation is generally thought to result in an untenable level of misclassifications of land versus water, and yet accurate manual interpretation and mapping of land–water boundaries is a labor-intensive solution (Sannel and Brown 2010) that limits regional-scale, remote-sensing-based permafrost monitoring, partly due to the variable quality of historical aerial photographs.

This paper demonstrates a semi-automated approach for using very-high-resolution imagery to quantify subtle landscape changes that are diagnostic of the health of near-surface permafrost in a wetland/tundra environment in the KOVA lowlands. We used high-precision co-registration techniques and active-contouring change-detection analysis to quantify water body surface area changes, and a difference-normalization approach to detect ice-wedge degradation during the periods between acquisition of early-1950s and late-1970s high- to very-high-resolution aerial photographs and post-2000 very-high-resolution optical satellite images. Change-detection analysis of more frequent but mid-resolution (Landsat) to high-resolution (SPOT) optical satellite imagery cannot identify ice-wedge degradation and

thus such image sources were not used in the analysis. Despite potential limitations of semi-automatic interpretation and mapping, such methods can expedite quantitative analysis of changes in subarctic ponds, lakes and adjacent polygonal terrain.

2. Site description

Kobuk Valley National Park is located in interior northwestern Alaska, USA, at 67°N (∼50 km north of the Arctic Circle). The low-lying Ahnewetut Wetlands study area (figure 1) is ∼170 km east of Kotzebue, Alaska. In this region, the Kobuk River lies within a hydrologic basin between the Baird and Waring Mountains to the north and south. Jorgenson *et al* (2008) suggested that the Kobuk River (figure 1) is an approximate dividing line between continuous permafrost to the north and discontinuous permafrost to the south where the Ahnewetut Wetlands are located. This is generally consistent with earlier mapping performed by Ferrians (1965), who indicated the region was just inside the demarcation boundary for continuous permafrost.

Ubiquitous ice-wedge polygons with scales ranging from <10 to 30 m, and subarctic ponds and lakes with scales

ranging from 0.2 to 1.5 km, lie at elevations of 9 to 46 m above mean sea level in Kobuk Valley; these features are evidence of the longstanding presence of permafrost in the basin (since at least the Late Glacial Maximum—locally the Walker Lake glaciation) and of local permafrost degradation (Fernald 1964, Hamilton 1982). As permafrost thaws, land subsidence occurs, developing topographic lows in which shallow thaw ponds and lakes may form (Hopkins 1949). While further degradation at the margins may initially increase water body size, continued permafrost degradation may ultimately lead to increased net infiltration and lake drainage if warming is not reversed.

The Ahnewetut Wetlands (figure 1) are a 14 000 ha, roughly triangular-shaped fluvial terrace bounded by the Kobuk River to the north, Ahnewetut Creek to the northwest, and Niaktuvik Creek to the southeast (Kuhry-Helmens *et al* 1985, Swanson 2001). The relatively smooth fluvial terrace is characterized by small, abandoned meandering fluvial channels in a polygonal peat plateau, and many shallow ponds and lakes (Kuhry-Helmens *et al* 1985). Regarding surface water bodies in Kobuk Valley, Fernald (1964, p K29) stated, 'Actively caving banks are generally 5–20 feet (1.5–6 m) high and commonly serrated where thawing proceeds more rapidly along ice-wedge polygons. The lakes in general show various stages of development. Some are being enlarged completely around their margins, but others are being filled where thawing and caving is no longer active. Some of the lakes have been partly emptied where an outlet to a lower level has been established. Many of the lakes are migrating through enlarging on one shore and filling on opposite shores'.

Today, many of the surface water bodies in the Ahnewetut Wetlands are associated with polygonal patterned ground of the intermediate-to-high-centered polygon type, with raised central polygons surrounded by subsided, trough-like networks of ice wedges. In contrast, these polygons were low-centered depressions commonly filled with ponds when aerial photographic image data were first collected during the mid-last-century. Shallow wetland ponds and lakes occur within lowland organic-rich loams and peat, and the surrounding ecosystems are dominated by bogs and fens or shrubs and forests (Jorgenson *et al* 2009). Larsen and Kristenson (2010) describe 5 representative lakes in this system that range in area from 2.6 to 17.3 ha, with a mean lake depth of 1.68 m and maximum depth ranging from 1.4 to 5.8 m. The case study domain (figure 2) ranges in elevation from 24 to 30.5 m above mean sea level; it accounts for less than 20% of the Ahnewetut Wetlands, but contains 7 of its 17 lakes larger than 20 ha.

The climate of Kobuk Valley is moderately continental (Hartman and Johnson 1984), subarctic and semiarid (mean annual precipitation 360 mm; Gibson 2009a) with cold winters (January mean: $-20.4\,^{\circ}$C) and warm summers (July mean: 15.4 $^{\circ}$C; Western Regional Climate Center 2011). Rainfall totals are significant from April to October, and precipitation peaks in August. Snowfall totals are not measured, but are included in 30-year gridded climate normals for Kobuk Valley precipitation (Gibson 2009a). Mean annual air temperature in Kobuk Valley was estimated to be (1) $-6\,^{\circ}$C
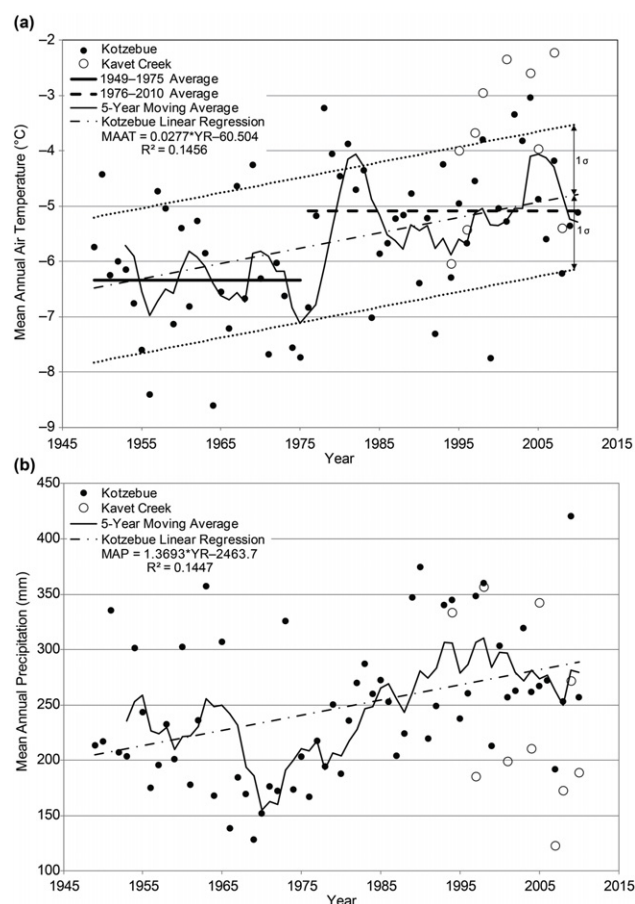

Figure 3. Climate data at Kotzebue, Alaska, since 1949 and at Kavet Creek, Alaska, since 1992. Data plotted for Kavet Creek are limited to those years with complete records. (a) Mean annual air temperature data from the Kotzebue NOAA station indicate this variable increased at a rate of $\sim$0.3 $^{\circ}$C/decade, perhaps with a step increase in 1976 at the onset of the last positive (i.e., warm) phase of the PDO. (b) Mean annual precipitation; erroneous data for Kavet Creek recorded in 1995 and 1996 were excluded. The Kavet Creek station only records liquid precipitation.

based on Ambler West climate station data for a site located 45 km east (Leslie 1989; cf Fernald 1964); (2) $-5\,^{\circ}$C by the 30-year gridded climate normals for Kobuk Valley air temperature for the period from 1971 to 2000 (Gibson 2009b); and (3) has been measured locally over the last 18 years to be $-4\,^{\circ}$C (Western Regional Climate Center 2011).

Relatively long climate records are available for the first-order meteorological station located in Kotzebue, Alaska (e.g., figure 3). In contrast, local weather data for KOVA, which are available from the Kavet Creek remote automated weather station (Western Regional Climate Center 2011), are limited to the period from 1992 to present (e.g., figure 3); this station is located $\sim$18 km from the study area at an elevation 72 m above mean sea level. Air temperature readings are available year-round, but neither cold-season precipitation nor snow depth is recorded. The Kavet Creek mean annual air temperature tends to be $\sim$1 $^{\circ}$C warmer than reported for Kotzebue (figure 3(a)). Mean annual air temperature (MAAT) records indicate a $\sim$1 $^{\circ}$C increase at Kotzebue since 1975
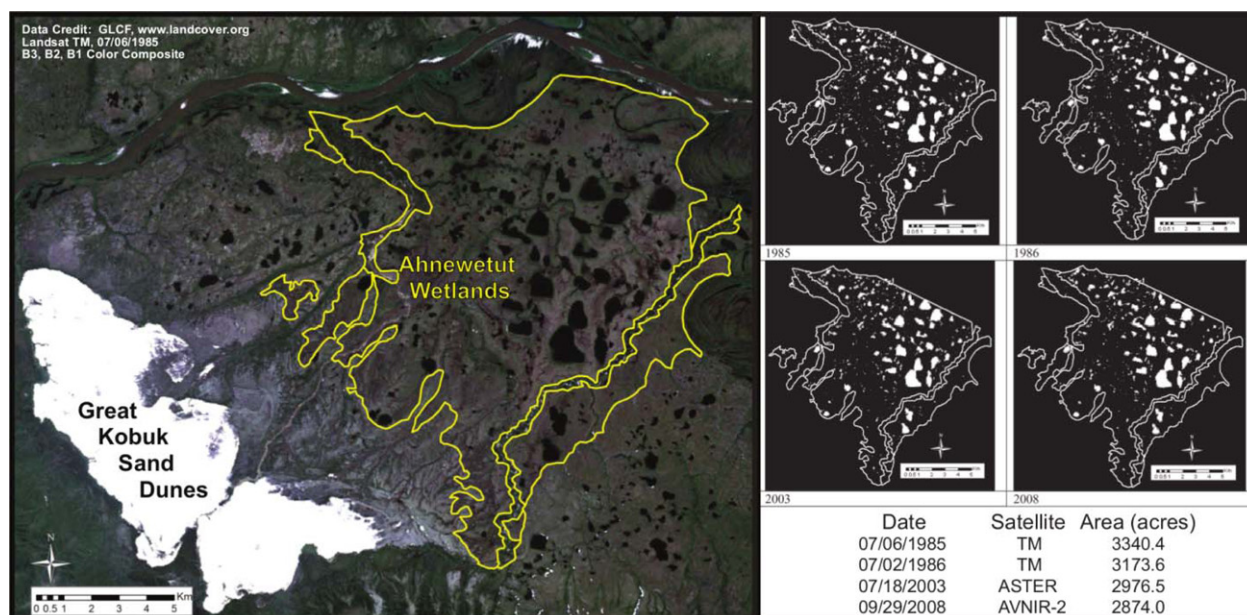
Figure 4. Preliminary work used unsupervised classification of mid-resolution Landsat Thematic Mapper, Advanced Spaceborne Thermal Emission and Reflection radiometer (ASTER), and Advanced Visible and Near Infrared Radiometer type 2 (AVNIR-2) satellite data to reveal system-wide downward trends in surface water area between the years 1985 and 2008. During this period, 14% of the estimated 1985 surface water area was lost.

and possibly a similar increase at Kavet Creek. Mean Annual Precipitation (MAP) has also increased since 1975. These changes coincided with a transition from a cool to warm phase of the Pacific Decadal Oscillation (PDO) in 1976 (Mantua 2012).

During early work, Necsoiu *et al* (2009a) performed unsupervised classification on Landsat TM, ASTER (Advanced Spaceborne Thermal Emission and Reflection Radiometer), and ALOS AVNIR-2 (Advanced Land Observing Satellite— Advanced Visible and Near Infrared Radiometer-2) imagery spanning the years 1985–2008, and quantified surface water areal changes within the Ahnewetut Wetlands (figure 4). This preliminary analysis estimated a 14% decrease in water surface area within the wetlands, mainly associated with smaller water bodies. The largest 25 lakes in the wetlands had a consistent number of water pixels in the analysis, which suggested little change in wetted lake area during this 23-year period, but the mid-resolution satellite images may have masked changes in shoreline geometry. Larger lakes are able to maintain their size via wave-cut erosion (long fetch translates to high potential wave energy; Sannel and Kuhry 2011) and thaw slumping (large water bodies have higher heat capacities than smaller water bodies).

Recognizing the possible limitations of fully automated classification methods (e.g. Sannel and Brown 2010), we have pursued new semi-automated methods to detect and quantify very small changes in these same surface water bodies and associated polygonal terrain using high-resolution imagery, high-precision orthorectification and co-registration, active-contouring techniques, and a normalized difference index. These analyses span 1951–2005, nearly the entire period of record for this wilderness area.

3. Data and methods

Lake shorelines have a fractal nature (e.g., Mandelbrot 1967) and their apparent length scale depends on image resolution. The image data used in this analysis were three 1951 black and white (B/W) aerial photographs, a 1978 color infrared (CIR) aerial photograph, a 2005 high-resolution Quickbird satellite image, and two 2008 ALOS PRISM (Advanced Land Observing Satellite Panchromatic Remote-sensing Instrument for Stereo Mapping) images. The B/W aerial photographs were acquired on 26 August 1951 by the US Navy KBV project. The CIR aerial photo was acquired by NASA's Johnson Space Center, project 386, on 5 July 1978. The satellite image is a panchromatic dataset acquired by DigitalGlobe on 18 August 2005 with a resolution of 0.68 m. Two ALOS PRISM images from an image triplet acquired on 29 September 2008 were used to derive a 2.5 m resolution digital surface model (DSM) essential to the orthorectification and co-registration process. Image numbers and camera details are provided in the online supplementary data and methods (available at stacks.iop.org/ERL/8/025007/mmedia).

3.1. Orthorectification and co-registration

High-precision orthorectification and co-registration of these images was performed using the COSI-Corr (Co-registration of Optically Sensed Images and Correlation) technique (Leprince *et al* 2007b) with the 2005 satellite image as the reference. The potential and limitations of this technique have been demonstrated by several studies using satellite-based remote sensing data; these studies included measurement of glacier-surface velocities in mountainous terrain (Scherler *et al* 2008, Herman *et al* 2011), co-seismic deformation
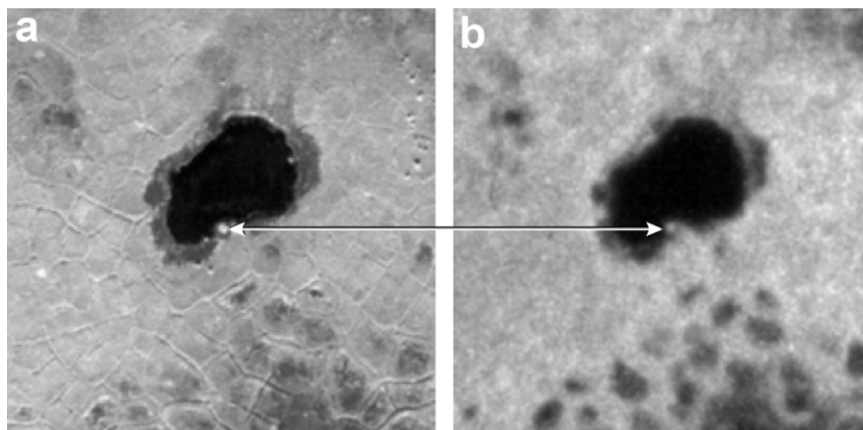
Figure 5. Example of a relatively stable feature (diameter 2.6 m) used as a tie point to precisely co-register remotely sensed imagery. (a) 2005 master image; (b) 1951 slave image.

(e.g., Avouac *et al* 2006, Copley *et al* 2011), and sand dune migration (e.g., Vermeesch and Drake 2008; Necsoiu *et al* 2009b; Bandeira *et al* 2011). Only two studies previously applied the COSI-Corr technique to aerial imagery: Leprince *et al* (2007a) and Ayoub *et al* (2009) used US Geological Survey—National Aerial Photography Program aerial data in conjunction with satellite data to analyze the co-seismic deformation associated with the 1992 Landers, California, earthquake.

For this study, the film-based aerial images were scanned with high spatial and radiometric resolution to accurately retrieve their information. Orthorectification and co-registration were performed as described by Leprince *et al* (2007a) with minimum available information (i.e., scanning resolution, fiducial points coordinates, principal point assumed to be at the crossing of the lines joining the opposite fiducial points) to set the camera geometry.

Preliminary work (Necsoiu *et al* 2010a, 2010b) revealed that even though the aerial photographs had correct quantification, co-registration was problematic because of scarcity of stable tie points. In addition, intrinsic factors such as (a) camera geometry and radial and tangential lens distortions, (b) spatial and radiometric resolution, (c) atmospheric diffraction, and (d) scratches and artifacts are major hindrances to obtaining satisfactory results in registering aerial datasets (Ayoub *et al* 2009, Necsoiu *et al* 2010b).

These issues were addressed by carefully identifying, selecting and optimizing (i.e., through several iteration loops) stable tie points from the few available relatively stable landscape features. Eight tie points were selected from flat regions of the DSM to anchor the 1951 aerial photo to the 2005 satellite image, and most tie points coincided with relatively stable palsas (figure 5). The resulting average misregistrations were only a few centimeters (e.g., $\sim$0.02 $\pm$ 0.74 m for a B/W image and $\sim$0.05 $\pm$ 1.09 m for the CIR image).

3.2. Polygonal terrain analysis

Multi-temporal image analysis of recent changes in the morphology of polygonal terrain is in its infancy; this is one of the first papers to provide a broadly applicable methodology—the normalized difference index—to address the topic. Simple image comparison techniques such as blending/fading, swiping, blinking or flickering are effective for quick visualization of visible changes in ice-wedge polygons, but quantification of morphological change requires a more sophisticated approach. Before implementing a change-detection analysis of polygonal terrain (such as quantification of polygonal joint width), the following conditions should be satisfied (Lu *et al* 2004).

(1) Precise co-registration of multi-temporal images.
(2) Precise radiometric and atmospheric calibration or normalization between multi-temporal images.
(3) Similar phenological states between multi-temporal images.
(4) Selection of the same spatial and spectral resolution images, if possible.

Ideally each dataset will require *a priori* standardization by normalizing image pixel values for differences in sun illumination geometry, atmospheric effects and instrument calibration. For our case study, lack of camera calibration data made absolute standardization of the aerial data impossible. Instead, assuming that the relationship between the radiance obtained by sensors from regions with constant reflectivity could be approximated by a linear function, a relative radiometric normalization of the datasets was performed via a statistical adjustment approach (Mena and Malpica 2009). The recent 2005 satellite image was used as the reference because it had the best visual quality and the largest dynamic range, maximizing retention of available information (Lo and Yang 1998). The relatively high resolution historical 1951 image was used in the bi-temporal analysis, whereas the low resolution of the historical 1978 image was deemed insufficient for quantitative analysis (figure 6).

To qualitatively and quantitatively identify changes, a normalized difference index (NDI) was calculated as:

$$\mathrm{NDI} = \frac{\mathrm{NB_{norm}(recent) - NB_{norm}(historical)}}{\mathrm{NB_{norm}(recent) + NB_{norm}(historical)}}$$
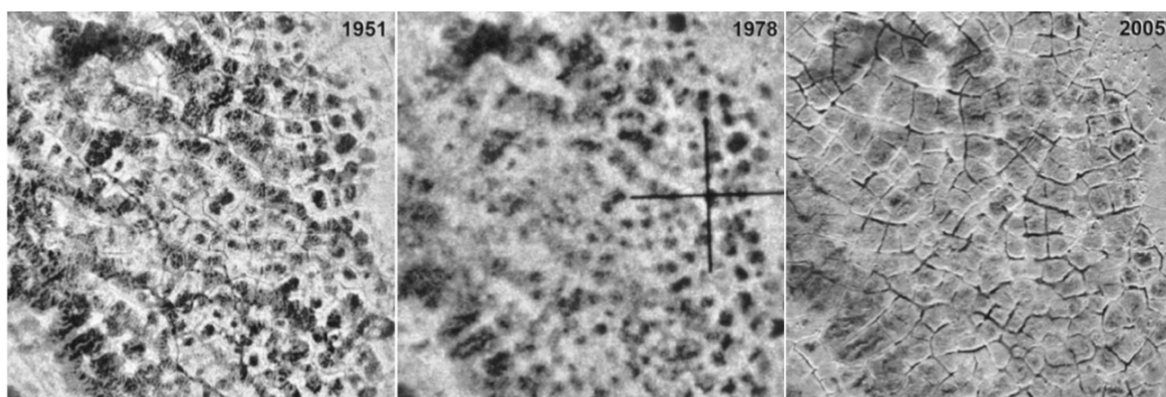
Figure 6. Enhanced tri-temporal images of polygonal terrain (1951, 1978, 2005). See figure 2 for context.
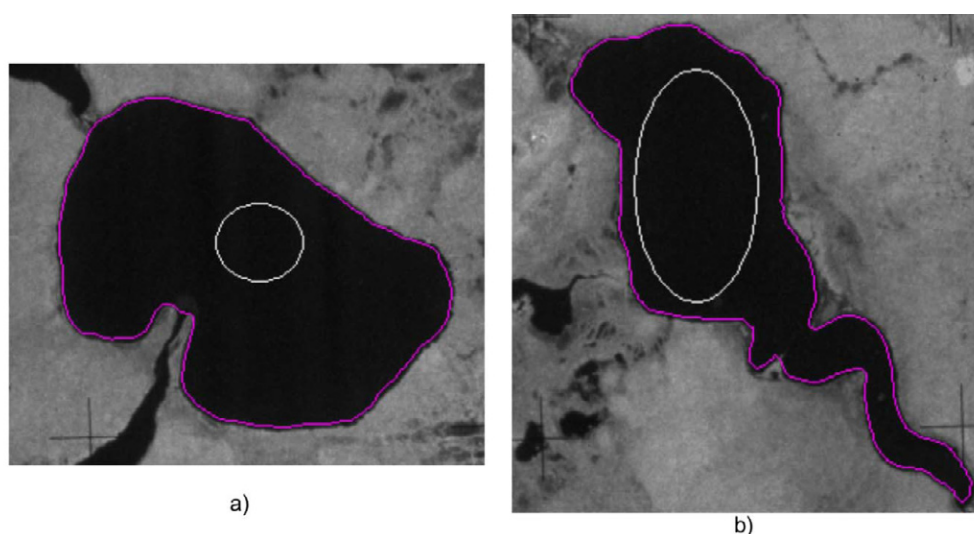

Figure 7. Starting from a seed oval or snake (white), lake boundaries (purple) are successfully retrieved. See figure 2 for context.

where NB is the normalized brightness of each pixel. NDI is a particular case of the normalized difference reflectance or NDR, an index introduced by Villa *et al* (2009) to assess bi-temporal land cover changes by exploiting the entire spectral range of panchromatic, multispectral and hyperspectral images. As with NDR, NDI follows a difference-normalization approach, introduced in remote sensing for vegetation studies with the normalized difference vegetation index (Kriegler *et al* 1969). NDI was calculated with the 1951 dataset normalized to the 2005 dataset for the image area shown in figure 7, which consists of 500 pixels × 500 pixels (∼310 m × 310 m). Using NDI, a preliminary assessment of changes in moisture, identified as an increase or reduction in brightness, was performed without information loss, in contrast to other change-detection techniques such as indices, compression or feature reduction. NDI ranges from −1 to +1, where −1 indicates maximum reflectance decrease, 0 is no change, and +1 indicates maximum reflectance increase. A threshold NDI of −0.6 was used to illustrate low-lying polygonal joints in which wedge ice had melted; likewise, a threshold of +0.6 was used to illustrate land that had become relatively high and dry. These selected thresholds were based upon image interpretation and professional judgment in consultation with David Swanson (US National Park Service).

3.3. Water body surface area analysis

Using the 1951, 1978, and 2005 image data, a series of algorithms were applied to define water body surface area changes in Ahnewetut Wetlands; 7 ponds (initially 0.09–0.5 ha) and 15 lakes (initially 2–180 ha) were assessed. All lakes in the study area larger than 2 ha were assessed, but fewer than half the ponds were considered (figure 2).

　　The quantitative solution for assessing water body surface area change consisted of (1) a data-clustering algorithm with nonparametric density gradient estimation (Fukunaga and Hostetler 1975); (2) a Canny–Deriche edge-detection algorithm (Deriche 1987) to identify the shoreline (this commonly used algorithm is not discussed further); and (3) an active-contouring 'snake' algorithm (based on a deformation model originally proposed by Boudier 1997) to contour the shoreline.
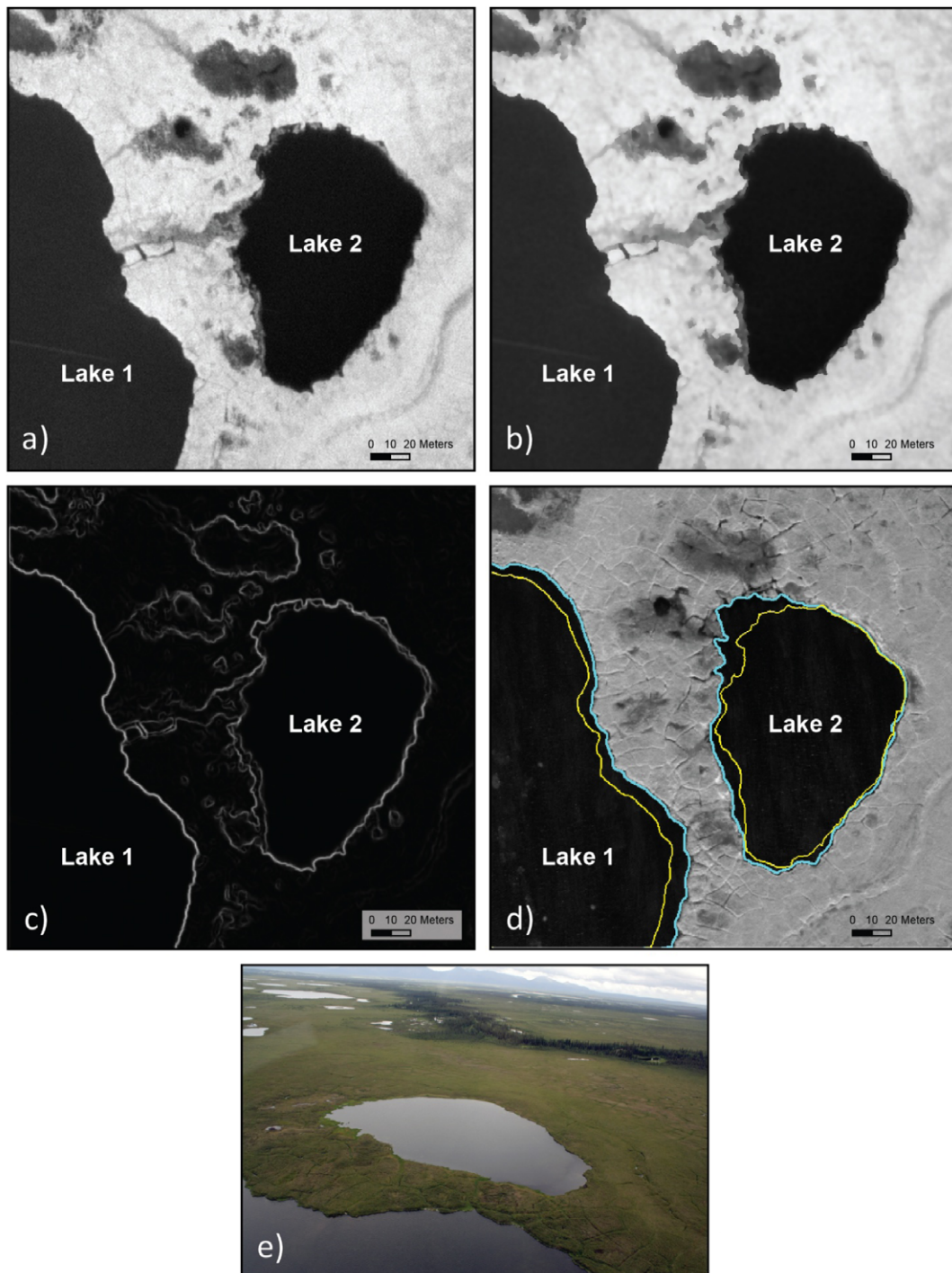
Figure 8. Change detection illustrated within a small 375 m × 375 m test area. See figure 2 for context. (a) The 1951 aerial photograph; (b) output of the data-clustering algorithm; (c) output of the Canny–Deriche edge-detection algorithm; (d) result of active contouring applied to the 1951 (yellow contours) and 2005 (cyan contours) images, overlaid on the 2005 image; cuspate shoreline features indicate preferential erosion along polygonal joints; (e) oblique aerial photograph of the narrow land bridge between Lake 1 and Lake 2 (acquired 12 July 2011).

The nonparametric estimator of density gradient, essential to preprocessing, was used as a discontinuity-preserving filter. Using it, the set of pixels within a spatial radius and defined gray distances for each pixel were determined. Based on this set of neighboring pixels, a new spatial center and mean gray value was computed. The calculated mean values serve as the center for the next iteration; iterations continue until the spatial and grayscale mean values stop changing (Barthel 2007).

Active contours (Kass *et al* 1988) are widely used in image processing for applications that include edge-detection object recognition, shape modeling and segmentation (Abrantes and Marques 1996, Boudier 1997, Terzopoulos and Fleischer 1988, Xu and Prince 1998, Comaniciu and Meer
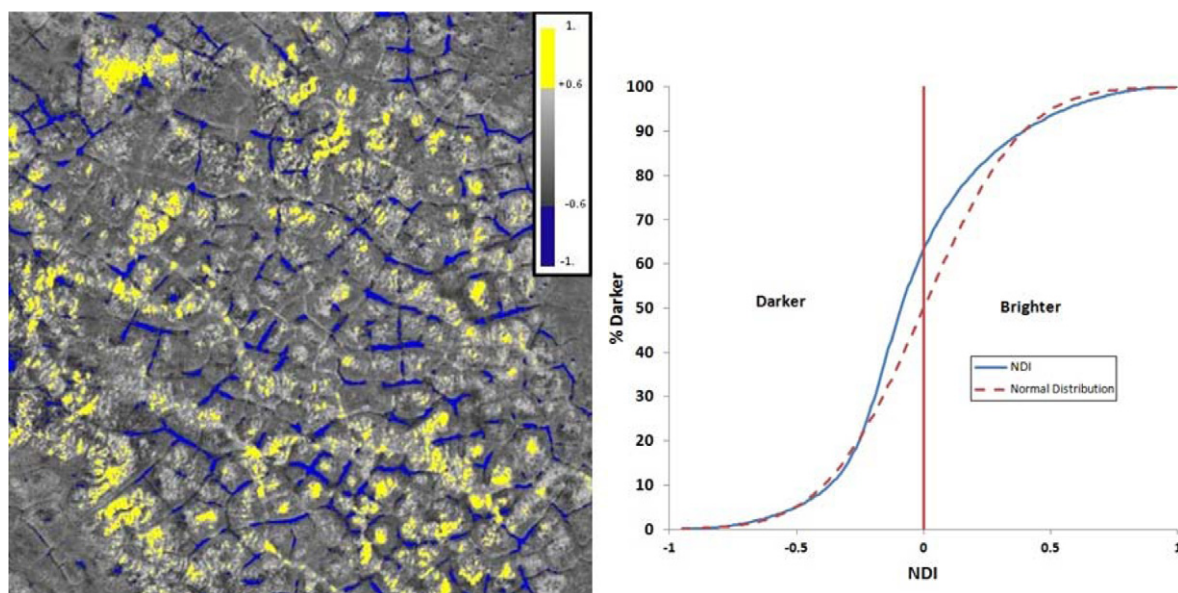
Figure 9. NDI values calculated based on the 1951 and 2005 images of figure 6 are shown superimposed on the 2005 image. Blue areas represent an NDI < −0.60 (i.e., change to relatively lower and wetter topography), and yellow areas represent an NDI > +0.60 (i.e., change to relatively higher and drier topography). The cumulative distribution of NDI values is similar to a normal distribution.

2002), to cite a few of many such studies. Active contours, or snakes, are curves defined within an image domain that can move under the influence of internal forces coming from within the curve itself and external forces computed from the image data (Xu and Prince 1998).

Our method uses a geometric active-contouring technique developed by Boudier (1997) that circumvents elasticity constraints and the gradient-based driving forces that prevent mapping embayments (Andrey and Boudier 2006).

Compared with traditional active-contouring algorithms, this implementation can (1) start far from water body boundaries and converge to boundary concavities, or (2) start near some boundaries while being far from others, yet still converge to boundary concavities. The active-contouring algorithm is initiated by manually creating a seed oval or polygon snake within the water body image feature (figure 7). A polygonal seed may be defined for water bodies having complex geometry or affected by emergent vegetation with shallow shorelines. The algorithm concludes when the snake has expanded to positions adjacent pixels used as the edge threshold, resulting in a bounding contour that is shifted approximately one pixel inside the water body image feature (figure 7). This systematic shift yields water body area estimates that could be slightly smaller than if manually digitized, but these estimates are objective and consistent between water bodies and images, unlike manual digitization estimates. The image processing sequence is illustrated in figure 8.

4. Results

4.1. Polygonal terrain

Precise orthorectification and co-registration revealed significant changes in the morphology of ice-wedge polygons. The

1951 and 1978 images (figure 6) suggest that low-centered ice-wedge polygons and polygonal pools were relatively stable between 1951 and 1978. The 2005 image suggests that since 1978, within only three decades, polygonal joints consisting of melting ice wedges have subsided considerably relative to the newly high-standing centers of polygonal peat plateaus (figure 6, cf Jorgenson *et al* 2006).

The results of the quantitative bi-temporal NDI analysis are illustrated in figure 9. Blue areas with NDI values less than −0.6 represent polygonal joints that had lower brightness values, consistent with relatively wet, melting wedge ice. Yellow areas with NDI values greater than 0.6 represent land that had became brighter, consistent with relatively dry, high-centered polygons. Overall, these observations are consistent with a transformation from low-centered to intermediate-to-high-centered polygons between 1951 and 2005. Although the cumulative distribution of NDI values approximates a normal distribution (dashed curve), ~63% of the area had lower brightness values (figure 9). Using the ±0.6 NDI thresholds, troughs of melted wedge ice account for ~3% of the 2005 image area, whereas polygonal centers that became drier account for ~4% of the image area.

Similar changes are shown in figure 10, which illustrates a classic example of ice-wedge degradation. Thermokarst pits that formed within a birch forest (D in figure 10; see Jorgenson and Osterkamp 2005 and Jorgenson *et al* 2010) either were not present in 1951 or were too small to be visible. Microtopography changed from that dominated by low-centered polygons in 1951 to intermediate-to-high-centered polygons in 2005.

4.2. Water body surface areas

The shorelines of 22 water bodies were defined for each image, and per cent change in surface area for each time
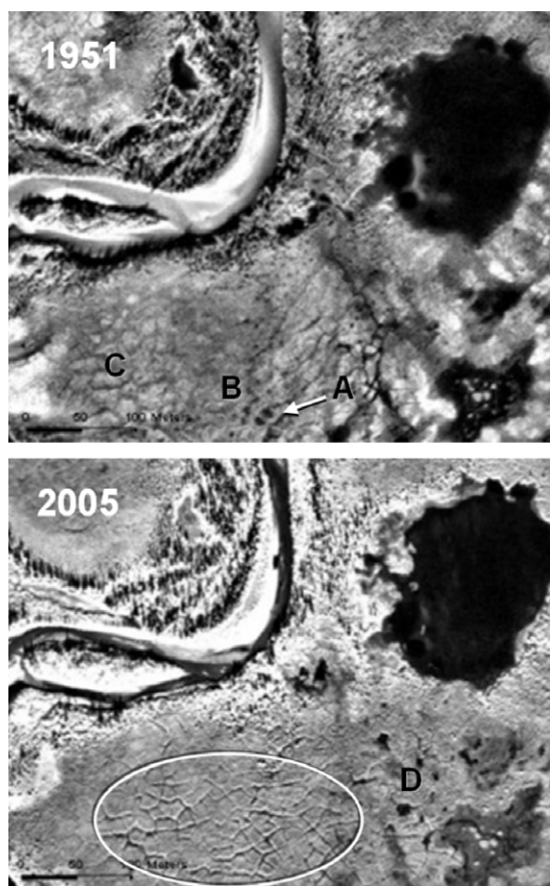
Figure 10. Ice-wedge degradation illustrated; see figure 2 for context. The 1951 image shows low-centered polygons at A (dark centers indicate wetness), indistinct polygons at B (probably flat), and slightly high-center polygons at C (polygon margins are darker, probably a bit wetter than the centers). The land area within the ellipse in the 2005 image illustrates permafrost degradation: the polygonally jointed network is producing shadows because the surface has a network of deep troughs where near-surface massive ice used to be. Area D illustrates development of typical thermokarst pits by 2005 from surface thawing that were either smaller or not present in 1951. The pits appear to have formed on a recently abandoned floodplain; note a highly connected jointed network of subsided ice-wedge troughs in this region—clearly evident in the 1951 aerial photograph but indistinct and replaced with thermokarst pits by 2005.

period were computed (figure 11, table 1). For those who wish to compare these results against those of other studies that restricted analyses to lakes exceeding a certain size threshold, of the water bodies analyzed, seven were ponds smaller than 0.5 ha, seven were lakes ranging from 2 to 8 ha, four were lakes ranging from 13 to 28 ha, and four were large lakes in excess of 40 ha (figure 12, table 1). Water body surface area trajectories are shown in figure 12 as cumulative per cent change since 1951 versus surface area.

Little change was detected during the 1951–78 timeframe with the exceptions of Lake 2, which increased in surface area by 15%; Lake 15, which decreased in surface area by 17%; and Pond 6, located at the edge of a meander bend where drainage by stream piracy may have played a role, catastrophically decreased in surface area (figures 11, 12

and table 1). The net water body surface area across the study domain was essentially stable during this early period (table 1), with large relative losses in small ponds balanced by small relative increases in large lakes (figure 12). Significant decreases in surface area of most shallow ponds occurred between 1978 and 2005; Ponds 4 and 6 went dry (table 1 and figure 12).

Lake 18 expanded slightly during the first period and contracted equally during the second period (table 1 and figure 12). Four lakes occupying a local basin in the western part of the study domain decreased in surface area (Lakes 14, 15, 21, and 22); Lakes 14, 21 and 22 are linked by incised channels that drain to the north (figure 12, inset). Two lakes greater than 25 ha (Lakes 20 and 21) experienced a significant decrease in surface area (table 1 and figure 12); Lake 20 occupies a local topographic high in contrast to basin-bound Lake 21. Water body surface area losses tended to be focused within (1) 'highland' ponds near Niaktuvik Creek and (2) basin-bound lowland lakes linked by incised channels. Three lakes greater than 40 ha (Lakes 1, 10 and 11) slightly increased in surface area throughout the 54-year period of record (table 1). Arctic lakes larger than this threshold are relatively stable in response to perturbations (Smith *et al* 2005, and their online supplementary material). Overall, 12 of 22 water bodies (10 lakes and 2 ponds) were relatively stable with net surface area decreases of ≤10% whereas 10 water bodies (5 lakes and 5 ponds) exhibited surface area losses in excess of 10% (figure 12). The net change in water body surface area within the study domain was −5.9% (table 1).

Although orthorectification and co-registration are not required to measure changes in water body surface areas, they are required to measure lateral migration rates of lakes using the active-contouring method. Subtle changes were noted along the western shore of Lake 1 (informally named Child Lake, figure 13), including (1) shoreline advancement as emergent vegetation colonizes shallow water (vegetated area between yellow and cyan contours) and (2) very limited lake expansion. In stark contrast, differential eastward expansion of Lake 1 is apparent by inundation observed along its eastern shoreline (inundated area between yellow and cyan contours). Lake 1 likely expanded along ice-wedge exposures on the steeper/deeper shorelines (i.e., along much of the northern, eastern, and southern shores) by thaw slumping or wave-cut erosion (cf Pelletier 2005). Preferential eastward shoreline expansion may be in response to (1) differential insolation during the heat of the day when the sun is in the western sky or (2) frequent westerly winds that occur in open water season. The rate of erosion averaged over 54 years varies from less than ∼0.03 m yr^{-1} (i.e., the co-registration accuracy of the method) to ∼0.5 m yr^{-1} (<∼0.3 to ∼5 m/decade). The ∼5 m/decade erosion rate is similar to the 7.3 m/decade lateral expansion rate calculated by Sannel and Kuhry (2011) for a lake in the Hudson Bay lowlands at the southernmost boundary of the continuous permafrost zone; peat thickness is considerably greater at the Hudson Bay location (1.5 m compared to 0.5 m adjacent to Lake 1) and mean annual air temperatures are ∼2 °C cooler.

Lake 2 (figure 13) shows preferential westward and northwestward expansion (figure 12 and table 1) in the
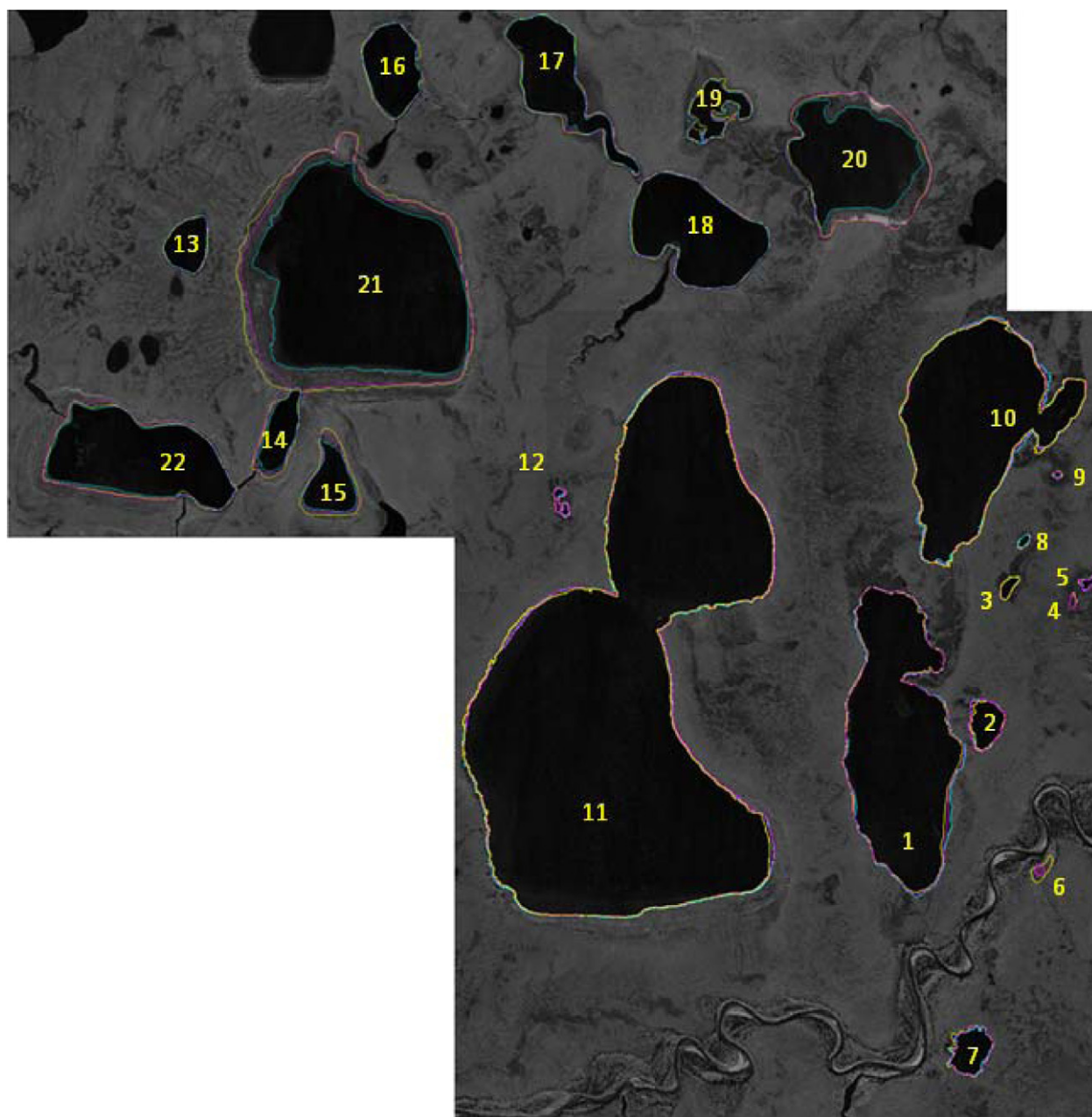
Figure 11. Panchromatic 2005 DigitalGlobe image draped with water body surface area contour lines estimated for three imagery dates. Yellow—1951, magenta—1978, cyan—2005. See figure 2 for context.

direction of Lake 1 (figure 8(d)) suggesting that the peat plateau between the water bodies is susceptible to permafrost degradation. Based on field characterization, soil appears to erode along the lake margin, becomes entrained in the water, and is redeposited on the eastern edge of this small lake where newer margins are observed. In the absence of field data, these shoreline changes would not have been apparent using lower resolution images or without precise image co-registration. At the maximum rate of advancement, and given that the land bridge is 30–100 m wide, these lakes may coalesce in as few as 30 years if the ground temperature of the land bridge warms while the land area declines.

　　　Challenges specific to surface-water-body-change analysis include the presence of emergent vegetation, shallow

shorelines, and opacity of sediment discharge areas (cf Riordan *et al* 2006, Sannel and Brown 2010) because affected areas produce reflection values similar to those of bare soil. The active-contouring algorithm may underestimate lake area when faced with complicating factors like these, necessitating human-in-the-loop interpretation.

5. Discussion and conclusions

The wetlands in KOVA are remote and relatively untouched by humankind, which suggests that ongoing permafrost degradation in the region is a result of climatic factors that are disturbing the ground thermal regime, whether short-term

Table 1. Water body surface areas and per cent change.

Lake/pond no.	Area (ha)			% change[a]		
	1951	1978	2005	1978/1951	2005/1978	2005/1951
1	43.64	44.5	45.3	1.97	1.80	3.80
2	2.16	2.48	2.43	14.81	−2.02	12.50
3	0.43	0.44	0.43	1.61	−3.39	−1.84
4[b]	0.13	0.12	0.00	−7.69	−100	−100
5	0.26	0.25	0.20	−3.85	−20.00	−23.08
6[b]	0.49	0.11	0.00	−77.55	−100	−100
7[c]	2.94	2.73	2.61	−7.14	−4.4	−11.22
8	0.19	0.19	0.18	0.00	−5.26	−5.26
9	0.09	0.09	0.06	0.00	−33.33	−33.33
10	43.96	44.35	44.97	0.89	1.40	2.30
11	179.10	180.30	181.15	0.67	0.47	1.14
12	0.41	0.39	0.35	−4.88	−10.26	−14.63
13	3.48	3.50	3.57	0.48	2.07	2.57
14	4.62	4.47	3.75	−3.26	−16.18	−18.91
15	5.96	4.94	4.46	−17.15	−9.61	−25.10
16	7.82	7.51	7.53	−4.00	0.31	−3.70
17	13.15	13.05	12.75	−0.76	−2.32	−3.06
18	19.99	20.10	19.98	0.53	−0.58	−0.05
19[c]	3.99	3.98	3.97	−1.35	0.83	−0.53
20	27.48	28.25	20.57	2.81	−27.20	−25.15
21	83.16	78.93	63.01	−5.09	−20.17	−24.23
22[d]	24.7	25.75	23.31	4.25	−9.50	−5.65
Total area (ha)	468.16	466.38	440.57	−0.4[e]	−5.5[e]	−5.9[e]

[a] Per cent change between subsequent images is based upon the water body surface area of the preceding image; therefore, the overall per cent change is not necessarily the sum of the per cent changes of the 1978/1951 and 2005/1978 pairs.
[b] Pond dried completely by 2005.
[c] Lake geometry issues resulted in considerable uncertainty.
[d] Difficult to define the shore in the W, NW, and N sides of the lake.
[e] Per cent change in total water body surface area.

seasonal variability, the multi-decadal PDO, anthropogenic climate change, or some combination thereof. While the PDO switched from a negative (cool) to positive (warm) phase ∼2 years before the 1978 image was acquired, some minimal lag time might be expected between the onset of enhanced thermal forcing associated with the new warm phase of the PDO and quantifiable morphological changes evident in imagery. Thus, it is fortuitous that the limited imagery available for this analysis is so well-matched to the 1976 PDO inflection point. Locally varying antecedent conditions, including lithology, ground ice distribution, hydrology, water body volume, vegetation, slope aspect and topography affect local active layer, snow, and ice thicknesses and the ground thermal regime—causing disparate evolutionary trajectories of water bodies within a single wetland; some bodies expand while others contract or drain completely when a local, critical threshold of instability is met (Marsh *et al* 2009). The observed decreases in small pond surface area while several large lakes exhibited slight growth is consistent with the understanding that ponds are more sensitive than large lakes to thermal perturbations; nevertheless, several large lakes had significant declines in surface area.

The total water body surface area across the study domain was essentially stable from 1951 to 1978 (figures 11 and 12), decreasing only 0.4% (table 1) during a relatively cool climate period (figure 3), with large relative losses

in small ponds offset by small relative increases in large lakes. However, during the subsequent interval from 1979 to 2005—associated with a relatively warm climate and increased MAP (figure 3)—total water body surface area decreased by 5.5% (table 1), 16 of 22 water bodies exhibited decreased surface area, and polygonal terrain morphology evolved from low-centered polygons to intermediate-to-high-centered polygons. Overall, 12 of 22 water bodies (10 lakes and 2 ponds) were relatively stable with net surface area decreases of ≤10%, including 4 lakes that gained area during both time intervals; however, 10 of 22 water bodies (5 lakes and 5 ponds) had surface area losses in excess of 10%, including 3 lakes and 2 ponds with losses in excess of 20% and 2 ponds that drained completely.

Ice-wedge polygons observed in the Kobuk Valley lowlands near the present-day continuous permafrost zone boundary developed over hundreds to thousands of years. The low-centered polygons visible in the 1950s–70s aerial imagery may document well-preserved ice-wedge relics of a colder climate, but the intermediate-to-high-centered polygons observed in the 2005 satellite imagery illustrate that significant melt of wedge ice has occurred, which implies retreat of the permafrost table (Davis 2001), at least locally. Overall, the changes to polygonal terrain morphology that occurred between 1978 and 2005 represent a rapid
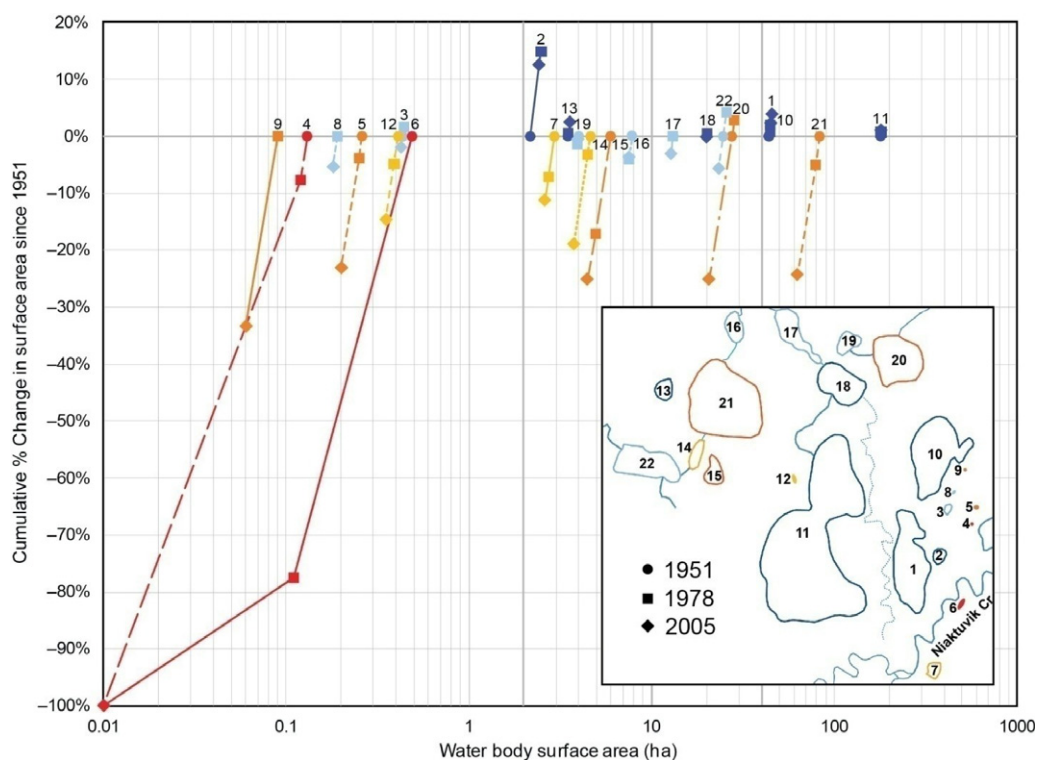
Figure 12. Scatterplot of cumulative per cent change in water body surface area since 1951 versus water body surface area. Circle—initial state in 1951; square—per cent change over the 1951–78 period; diamond—per cent change over the 1951–2005 period of record. Dark blue—net surface area increase of $\geq 0\%$; light blue—net surface area decrease of $\leq 10\%$; yellow—net surface area decrease of $\leq 20\%$; orange—net surface area decrease of $>20\%$; red—catastrophic drainage. Typical lake analysis size thresholds are presented as vertical lines at 2, 10, and 40 ha. Inset water body map based upon Creely and Brabets (2000).

rate of permafrost degradation relative to generally accepted ice-wedge construction rates.

Co-registration of arctic images is particularly challenging due to a general lack of stable landmarks, but palsas may be relatively stable and therefore useful as tie points. Recognition of relatively stable landscape features during the timeframe of interest can yield a high-quality co-registration. The high-precision orthorectification and co-registration method and use of the normalized difference index for detecting changes in polygonal terrain is relatively fast to implement; thus, it has potential for use in production mode given an adequate supply of multi-temporal, very-high-resolution imagery over large regional areas. Multi-temporal analysis also can be used to identify, characterize and quantify expansion/contraction/migration of shallow, subarctic ponds and lakes to reveal important multi-decadal changes in arctic wetland geomorphology. The ability to accurately rectify and co-register aerial photographs and satellite imagery expands the time horizon over which changes in arctic landscapes can be analyzed.

Active-contouring change-detection methods used to objectively estimate water body surface areas can best be described as semi-automatic because they also involve human-in-the-loop preprocessing and interpretation. When quantifying lake migration, human intervention is needed during the co-registration step to identify stable tie points and during the initial stage of lake shoreline mapping to construct one rough shoreline polygon (i.e., 'snake') per lake to be

optimized during automated active contouring. Despite the potential limitations of semi-automatic methods, they can be used to expedite quantitative analysis of changes in subarctic ponds, lakes and adjacent polygonal terrain.

As water bodies drain and surface water is redistributed from polygon pools on the tundra to subsided polygonal troughs, wetland and aquatic habitat is rapidly converted to terrestrial habitat in the KOVA lowlands. Results from this remote sensing study can serve as baseline information about vital signs and decadal-scale vital-sign trends to inform strategic planning for monitoring the health and integrity of the KOVA wetlands. These analytical methods are also widely applicable to other conservation units in the region, and have widespread implications for management and wetland protection throughout northwestern Alaska. Semi-automated image analysis permits vital-sign quantification with respect to water body surface area and distribution, numbers of shallow ponds and lakes, and morphological indicators of permafrost characteristics.
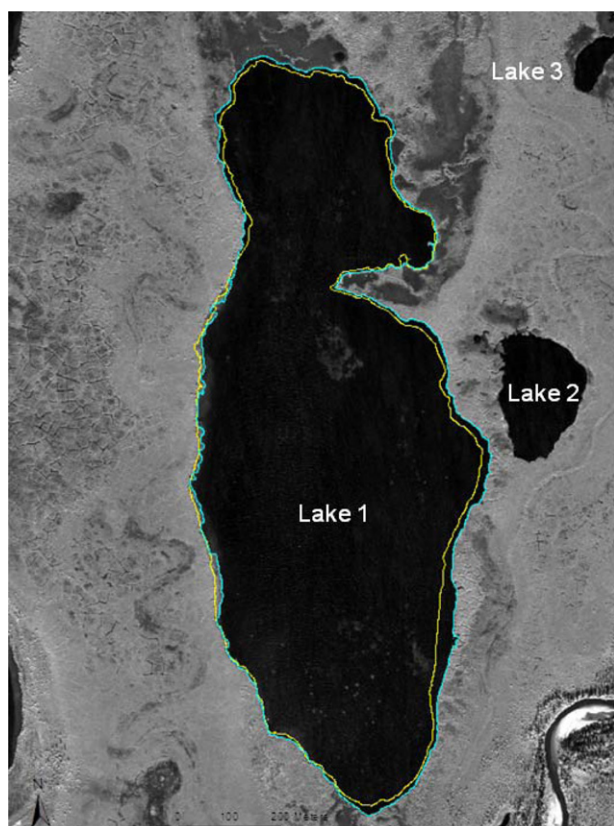
Acknowledgments

Figure 13. Lake 1 change detection (yellow—1951, cyan—2005);
see figure 2 for context. East and west of Lake 1, old, abandoned
meandering stream channels traverse terrain that generally has
indistinct to no visible polygons. Indistinct polygons may represent
an advanced stage of permafrost degradation where soil slumping
has infilled previously deeply thawed polygonal troughs (Jorgenson
and Osterkamp 2005), resulting in terrain leveling. Lake expansion
was greatest in 2005 at locations where polygonal troughs were
particularly deep and distinct. Where polygons are indistinct or
lacking, little lake expansion is observed. The northern third of Lake
1 appears to be surrounded by a drained, thermokarst basin,
suggesting it is currently smaller than its maximum extent and that
it may have been directly connected at one time to Lake 10
(figure 12) located due north. Topographic downgradient in the
image area is to the NNE.

References

Abrantes A J and Marques J S 1996 A class of constrained
clustering algorithms for object boundary extraction *IEEE
Trans. Image Process.* **5** 1507–21

Andrey P and Boudier T 2006 Adaptive active contours (snakes) for
the segmentation of complex structures in biological images
*Proc. 1st ImageJ User & Developer Conf. (Luxembourg, May
2006)* (http://imagejdocu.tudor.lu/lib/exe/fetch.php?
media=plugin:segmentation:active_contour:absnake.pdf,
4 September 2012)

Avouac J P, Ayoub F, Leprince S, Konca O and Helmberger D 2006
The 2005, Mw 7.6 Kashmir earthquake, rupture kinematics
from sub-pixel correlation of ASTER images and seismic
waveforms analysis *Earth Planet. Sci. Lett.* **249** 514–28

Ayoub F, Leprince S and Avouac J P 2009 Co-registration and
correlation of aerial photographs for ground deformation
measurements *ISPRS J. Photogramm. Remote Sens.* **64** 551–60

Bandeira L, Marques J S, Saraiva J and Pina P 2011 Automated
detection of Martian dune fields *IEEE Geosci. Remote Sens.
Lett.* **8** 626–30

Barthel K U 2007 *Mean Shift Filter* (http://rsbweb.nih.gov/ij/
plugins/mean-shift.html, 4 June 2012)

Berkes F and Jolly D 2001 Adapting to climate change:
social-ecological resilience in a Canadian Western Arctic
community *Conserv. Ecol.* **5** 18

Boudier T 1997 Elaboration d'un modèle de déformation pour la
détection de contours aux formes complexes *Innovat. Technol.
Biol. Méd.* **18** 1–13

Chapin F S III, Robards M D, Huntington H P, Johnstone J F,
Trainor S F, Kofinas G P, Ruess R W, Fresco N,
Natcher D C and Naylor R L 2006 Directional changes in
ecological communities and social-ecological systems: a
framework for prediction based on Alaskan examples *Am. Nat.*
168 S36–49

Comaniciu D and Meer P 2002 Mean shift: a robust approach
toward feature space analysis *IEEE Trans. Pattern Anal. Mach.
Intell.* **24** 603–19

Copley A, Avouac J P, Hollingsworth J and Leprince S 2011 The
2001 M(w) 7.6 Bhuj earthquake, low fault friction, and the
crustal support of plate driving forces in India *J. Geophys.
Res.—Solid Earth* **116** B08405

Creely E and Brabets T 2000 *COVERAGE KOBUK_9—
Hydrography—Kobuk River near Kiana—Gates of the Arctic
National Park and Preserve—Kobuk Valley National Park and
Preserve* (*Map Scale 1:63360*) (Anchorage, AK: US
Geological Survey) (geospatial data available at: www.agdc.
usgs.gov/, 29 January 2013)

Davis T N 2001 *Permafrost: A Guide to Frozen Ground in
Transition* (Fairbanks, AK: University of Alaska Press)

Deriche R 1987 Using Canny's criteria to derive a recursively
implemented optimal edge detector *Int. J. Comput. Vis.*
1 167–87

Fernald A T 1964 *Surficial Geology of the Central Kobuk River
Valley, Northwestern Alaska* (*Geological Survey Bulletin*
1181-K) (Washington, DC: United States Government Printing
Office)

Ferrians O J Jr 1965 *Permafrost Map of Alaska* (*US Geological
Survey Miscellaneous Geologic Investigations Map* I-445.
Scale 1:2 500 000) (Reston, VA: United States Geological
Survey)

Ford J and Bedford B L 1987 The hydrology of Alaskan wetlands,
USA: a review *Arct. Alp. Res.* **19** 209–29

Fukunaga K and Hostetler L 1975 The estimation of the gradient of
a density function, with applications in pattern recognition
IEEE Trans. Inf. Theory **21** 32–40

Gibson W 2009a *Mean Precipitation for Alaska 1971–2000*
(*Geospatial Dataset 2170508*) (Corvallis, OR: National Park
Service, Alaska Regional Office GIS Team) (PRISM data
available at: www.ocs.orst.edu/prism/stat_products/ak.maps.
html)

Gibson W 2009b *Mean Average Temperature for Alaska 1971–2000*
(*Geospatial Dataset 2170516*) (Corvallis, OR: National Park
Service, Alaska Regional Office GIS Team) (PRISM data
available at: www.ocs.orst.edu/prism/stat_products/ak.maps.
html)

Grosse G, Shirmeister L, Kunitsky V V and Hubberten H-W 2005 The use of CORONA images in remote sensing of periglacial geomorphology: an illustration from the NE Siberian Coast *Permafrost Periglac.* **16** 163–72

Hamilton T D 1982 A late Pleistocene glacial chronology for the southern Brooks Range: stratigraphic record and regional significance *GSA Bull.* **93** 700–16

Hartman C W and Johnson P R 1984 *Environmental Atlas of Alaska* (Fairbanks, AK: Institute of Water Resources and Engineering Experiment Station, University of Alaska at Fairbanks)

Herman F, Anderson B and Leprince S 2011 Mountain glacier velocity variation during a retreat advance cycle quantified using sub-pixel analysis of ASTER images *J. Glaciol.* **57** 197–207

Hinkel K M, Jones B M, Eisner W R, Cuomo C J, Beck R A and Frohn R 2007 Methods to assess natural and anthropogenic thaw lake drainage on the western Arctic coastal plain of northern Alaska *J. Geophys. Res.* **112** F02S16

Hinzman L D *et al* 2005 Evidence and implications of recent climate change in Northern Alaska and other Arctic regions *Clim. Change* **72** 251–98

Hopkins D M 1949 Thaw lakes and thaw sinks in the Imuruk Lake area, Seward Peninsula, Alaska *J. Geol.* **57** 119–31

Jones B M, Arp C D, Hinkel K M, Beck B A, Schmutz B A and Winston B 2009 Arctic lake physical processes and regimes with implications for winter water availability and management in the National Petroleum Reserve Alaska *Environ. Manag.* **43** 1071–84

Jones B M, Grosse G, Arp C D, Jones M C, Walter Anthony K M and Romanovsky V E 2011 Modern thermokarst lake dynamics in the continuous permafrost zone, northern Seward Peninsula, Alaska *J. Geophys. Res.* **116** G00M03

Jorgenson M T and Osterkamp T E 2005 Response of boreal ecosystems to varying modes of permafrost degradation *Can. J. Forest Res.* **35** 2100–11

Jorgenson M T, Romanovsky V, Harden J, Shur Y, O'Donnell J, Schuur E A G, Kanevskiy M and Marchenko S 2010 Resilience and vulnerability of permafrost to climate change *Can. J. Forest Res.* **40** 1219–36

Jorgenson M T, Roth J E, Miller P F, Macander M J, Duffy M S, Wells A F, Frost G V and Pullman E R 2009 An ecological land survey and landcover map of the Arctic Network *Natural Resource Technical Report* NPS/ARCN/NRTR-2009/270 (Fort Collins, CO: US National Park Service) p 307, + GIS database

Jorgenson M T, Shur Y L and Pullman E R 2006 Abrupt increase in permafrost degradation in Arctic Alaska *Geophys. Res. Lett.* **33** L02503

Jorgenson M T, Yoshikawa K, Kanevskiy M, Shur Y, Romanovsky V, Marchenko S, Grosse G, Brown J and Jones B 2008 Permafrost characteristics of Alaska *Proc. 9th Int. Conf. on Permafrost* pp 121–2

Kaab A, Haeberli W and Gudmundsson G H 1997 Analysing the creep of mountain permafrost using high precision areal photogrammetry: 25 years of monitoring Gruben rock glacier, Swiss Alps *Permafrost Periglac.* **8** 409–26

Kass M, Witkin A and Terzopoulos D 1988 Snake: active contour models *Int. J. Comput. Vis.* **1** 321–31

Kriegler F J, Malila W A, Nalepka R F and Richardson W 1969 Preprocessing transformations and their effects on multispectral recognition *Proc. 6th Int. Symp. Remote Sens. Environ.* pp 97–131

Kuhry-Helmens K F, Koster E A and Galloway J P 1985 Photo-interpretation map of surficial deposits and landforms of the Kobuk sand dunes and part of the Kobuk lowland, Alaska *US Geological Survey Open-File Report* 85-242, 1 sheet, scale 1:63,360

Larsen A S and Kristenson H 2010 Alaska shallow lake monitoring program: 2009 annual report *Natural Resource Data Series* NPS/AKRO/NRDS-2010/119 (Fort Collins, CO: National Park Service)

Leprince S, Ayoub F, Klinger Y and Avouac J P 2007b Co-registration of optically sensed images and correlation (COSI-Corr): an operational methodology for ground deformation measurements *IGARSS 2007: IEEE Int. Geosci. Remote Sens. Symp. (Barcelona)*

Leprince S, Barbot S, Ayoub F and Avouac J P 2007a Automatic and precise ortho-rectification, coregistration, and subpixel correlation of satellite images, application to ground deformation measurements *IEEE Trans. Geosci. Remote Sens.* **45** 1529–58

Leslie L D 1989 Alaska climate summaries: a compilation of longterm means and extremes at 478 Alaskan stations *Technical Note No. 5* 2nd edn (Anchorage, AK: Alaska Climate Center/Arctic Environmental Information and Data Center/University of Alaska at Anchorage)

Lo C P and Yang X 1998 Some practical considerations of relative radiometric normalization of multidate Landsat MSS data for land use change detection *Proc. American Society for Photogrammetry and Remote Sens. 1998 Annual Convention (Tampa, FL)* pp 1184–93

Lu D, Mausel P, Brondízio E and Moran E 2004 Change detection techniques *Int. J. Remote Sens.* **25** 2365–407

Mandelbrot B 1967 How long is the coast of Britain? Statistical self-similarity and fractional dimension *Science* **156** 636–8

Mantua N 2012 *PDO Index Monthly Values: January 1900–Present* (Seattle, WA: Joint Institute for the Study of the Atmosphere and Ocean, University of Washington) (data available at: www.jisao.washington.edu/pdo/PDO.latest, 9 December 2010)

Mars J C and Houseknecht D W 2007 Quantitative remote sensing study indicates doubling of coastal erosion rate in past 50 yr along a segment of the Arctic coast of Alaska *Geology* **35** 583–6

Marsh P, Russell M, Pohl S, Haywood H and Onclin C 2009 Changes in thaw lake drainage in the western Canadian arctic from 1950 to 2000 *Hydrol. Process.* **23** 145–58

Mena J B and Malpica J A 2009 A change detection method with radiometric normalization and shadows removal in multispectral satellite imagery (AMC-D-10-00861) (www2.uah.es/juan_mena/Publicaciones/change_detection.pdf, 4 June 2012)

Necsoiu M, Dinwiddie C L, Walter G R, Hooper D M and McGinnis R N 2009a Multispectral remote sensing technologies applied to assess recent aeolian activity and thaw lake changes in Kobuk River valley, Alaska *Presented at 2009 Fall Mtg (Dec.)* (San Francisco, CA: AGU) abstract U41C-0060

Necsoiu M, Hooper D M, Longépé N and Walter G R 2010a Monitoring subarctic permafrost changes using optical and multi-polarization SAR imagery *Presented at 2010 Fall Mtg (Dec.)* (San Francisco, CA: AGU) abstract EP51A-0538

Necsoiu M, Leprince S, Hooper D M, Dinwiddie C L, McGinnis R N and Walter G R 2009b Monitoring migration rates of an active subarctic dune field using optical imagery *Remote Sens. Environ.* **113** 2441–7

Necsoiu M, Longépé N and Walter G R 2010b Integrating remote sensing methodology for monitoring permafrost landscapes using ALOS satellite data *Proc. 4th ALOS Joint PI Symp. (Tokyo, Nov.)*

Osterkamp T E 2007 Characteristics of the recent warming of permafrost in Alaska *J. Geophys. Res.* **112** F02S02

Osterkamp T E and Romanovsky V E 1999 Evidence for warming and thawing of discontinuous permafrost in Alaska *Permafrost Periglac.* **10** 17–37

Pelletier J D 2005 Formation of oriented thaw lakes by thaw slumping *J. Geophys. Res.* **110** F02018

Plug L J, Walls C and Scott B M 2008 Tundra lake changes from 1978 to 2001 on the Tuktoyaktuk Penisula, western Canadian Arctic *Geophys. Res. Lett.* **35** L023502

Prowse T D, Wrona F J, Reist J D, Gibson J J, Hobbie J E, Levesque L M J and Vincent W F 2006 Climate changes effects on hydroecology of Arctic freshwater ecosystems *Ambio* **35** 347–58

Riordan B, Verbyla D and McGuire A D 2006 Shrinking ponds in subarctic Alaska based on 1950–2002 remotely sensed images *J. Geophys. Res.* **111** G04002

Roach J, Griffith B, Verbyla D and Jones J 2011 Mechanisms influencing changes in lake area in Alaskan boreal forest *Glob. Change Biol.* **17** 2567–83

Sannel A B K and Brown I A 2010 High-resolution remote sensing identification of thermokarst lake dynamics in a subarctic peat plateau complex *Can. J. Remote Sens.* **36** S26–40

Sannel A B K and Kuhry P 2011 Warming-induced destabilization of peat plateau/thermokarst lake complexes *J. Geophys. Res.* **116** G03035

Scherler D, Leprince S and Strecker M R 2008 Glacier-surface velocities in alpine terrain from optical satellite imagery—accuracy improvement and quality assessment *Remote Sens. Environ.* **112** 3806–19

Schindler D W and Smol J P 2006 Cumulative effects of climate warming and other human activities on freshwaters of arctic and subarctic North America *Ambio* **35** 160–8

Smith L C, Sheng Y, MacDonald G M and Hinzman L D 2005 Disappearing arctic lakes *Science* **308** 1429

Swanson D K 2001 *Ecological Subsections of Kobuk Valley National Park* (Anchorage, AK: Alaska Region Inventory and Monitoring Program, US National Park Service)

Terzopoulos D and Fleischer K 1988 Deformable models *Vis. Comput.* **4** 306–31

Vermeesch P and Drake N 2008 Remotely sensed dune celerity and sand flux measurements of the world's fastest barchans (Bodele, Chad) *Geophys. Res. Lett.* **35** L24404

Villa P, Lechi G and Gomarasca M A 2009 Multivariate differencing techniques for land cover change detection: the normalized difference reflectance approach *Geosci. Remote Sens.* ed P-G P Ho (Vienna: In-Tech) pp 277–300

Western Regional Climate Center 2011 *Kavet Creek Alaska (RAWS)* (Reno, NV: Western Regional Climate Center, Desert Research Institute) (data available at: www.raws.dri.edu/cgi-bin/rawMAIN.pl?akAKAV, 4 September 2012)

Xu C and Prince J L 1998 Generalized gradient vector flow external forces for active contours *Signal Process.* **71** 131–9

Yoshikawa K and Hinzman L D 2003 Shrinking thermokarst ponds and groundwater dynamics in discontinuous permafrost *Permafrost Periglac.* **14** 151–60